Switches, Catapults, and Chaperones: Steady-State Kinetic Analysis of Hsp70−Substrate Interactions†

Liudmila S. Chesnokova and Stephan N. Witt*

Department of Biochemistry and Molecular Biology, Louisiana State University Health Sciences Center, 1501 Kings Highway, Shreveport, Louisiana 71130-3932

Received April 28, 2005; Revised Manuscript Received June 20, 2005

ABSTRACT: Hsp70 chaperones are heterotropic allosteric systems in which ATP and misfolded or aggregated polypeptides are the activating ligands. To gain insight into the mechanism by which ATP and polypeptides regulate Hsp70 chaperone activity, the effect of a short peptide on the K_M for ATP was analyzed using the *Escherichia coli* Hsp70 called DnaK. In the absence of peptide, the K_M^{-P} for ATP is 52 ± 11 nM, whereas this value jumps to 14.6 ± 1.6 μM in the presence of saturating peptide. This finding supports a mechanism in which ATP binding drives the chaperone in one direction and peptide binding pushes the chaperone back in the opposite direction (and thus increases K_M), according to ATP + DnaK·P ⇌ ATP·DnaK·P ⇌ ATP·DnaK* + P, where ATP·DnaK·P is an intermediate from which competing ATP hydrolysis occurs (ATP·DnaK·P → ADP·DnaK·P). We show that this branched mechanism can even explain how DnaK hydrolyzes ATP in the absence of peptide and that the true rate constant for DnaK-mediated ATP hydrolysis (k_{hy}) in the absence of peptide may be as high as 0.5 s^{-1} (rather than 5×10^{-4} s^{-1} as often stated in the literature). What happens is that a conformational equilibrium outcompetes ATP hydrolysis and effectively reduces the concentration of the intermediate by a factor of a thousand, resulting in the following relation: $k_{cat} = k_{hy}/1000 = 5 \times 10^{-4}$ s^{-1}. How polypeptide substrates and the co-chaperone DnaJ modulate DnaK to achieve its theoretical maximal rate of ATP hydrolysis, which we suggest is 0.5 s^{-1}, is discussed.

The *Escherichia coli* Hsp70 molecular chaperone DnaK is an ATP-dependent molecular machine that functions to prevent and reverse the misfolding and aggregation of cellular proteins (for reviews, see refs *1*−*3*). Two co-chaperones, DnaJ and GrpE, regulate DnaK's activity. DnaJ, which is a chaperone itself, presents a substrate to DnaK and simultaneously signals DnaK to hydrolyze ATP, which finalizes substrate capture. GrpE is a nucleotide exchange factor that catalyzes the release of tightly bound ADP (*4*, *5*). The essence of the Hsp70 chaperone cycle is that the chaperone shuttles between an ADP-bound state, which has a high affinity for substrate proteins ($K_d \approx$ nanomolar) and an ATP-bound state, which has a low affinity for substrate proteins ($K_d \approx$ micromolar) (*6*, *7*). In each of these states, the nucleotides themselves, ADP and ATP, are tightly bound ($K_d \leq 200$ nM) (*8*, *9*). It is likely that DnaK utilizes free energy from ATP binding or hydrolysis to forcefully unfold substrates (*2*, *10*). In this sense, the DnaK/DnaJ/GrpE system is similar to the GroEL/ES system, which has been shown to fold substrates by forced unfolding (*11*).

DnaK consists of three domains: The 44-kDa nucleotide-binding domain (NBD),[1] the 12-kDa substrate-binding domain (SBD), and the 13-kDa multihelical lid domain comprise residues 1−384, 394−508, and 509−638, respectively. Residues 385−393, which are highly conserved among Hsp70s from different organisms, link the NBD to the SBD. With two lobes separated by a deep cleft in which nucleotide binds, the NBD binds and slowly hydrolyzes ATP (*12*). With a β-sandwich domain topped by a multihelical lid (*13*, *14*), the C-terminal domain binds and sequesters the substrate protein. A leucine-rich peptide (NRLLLTG), bound within the β-sandwich, makes numerous contacts via its main-chain atoms to side chains of DnaK residues that line the channel (*14*).

Hsp70 chaperones such as DnaK are heterotropic allosteric systems (*15*) in that ATP binds to the NBD, and this is sensed in the SBD, resulting in weakened peptide binding (*16*). Conversely, substrate binds to the SBD, and this is sensed by ATP lodged in the NBD, resulting in accelerated DnaK-mediated ATP hydrolysis (*17*). Although the structural changes that enable this interdomain communication are entirely mysterious, site-directed mutagenesis studies have revealed mutations in the NBD (E171A, D201N) (*18*, *19*), the highly conserved linker region (LL390,391DD) (*20*), and the SBD (K414I, N451K) (*21*) that either lower or abolish

† This work was supported in part by a grant from the National Institutes of Health (GM 51521) and the Stiles Foundation of LSUHSC-Shreveport.

* To whom correspondence should be addressed: Tel: (318) 675−7891. Fax: (318) 675−5180; e-mail: switt1@lsuhsc.edu.

[1] Abbreviations: NBD, nucleotide-binding domain; HEPES, *N*-(2-hydroxyethyl) piperazine-*N*′-2-ethanesulfonic acid; p5, the synthetic peptide CLLLSAPRR; SBD, substrate-binding domain; ADP·DnaK, "high affinity" state because it tightly binds substrate polypeptides; ATP·DnaK*, "low-affinity" state because it weakly binds substrate polypeptides; ATP·DnaK·P, an intermediate; $_c$DnaK, an isomer in which the ATPase domain is closed; and $_o$DnaK, an isomer in which the ATPase domain is open. "·", represents a noncovalent interaction, such as a peptide molecule, P, bound to DnaK (DnaK·P).

10.1021/bi050787b CCC: $30.25
Published on Web 07/14/2005

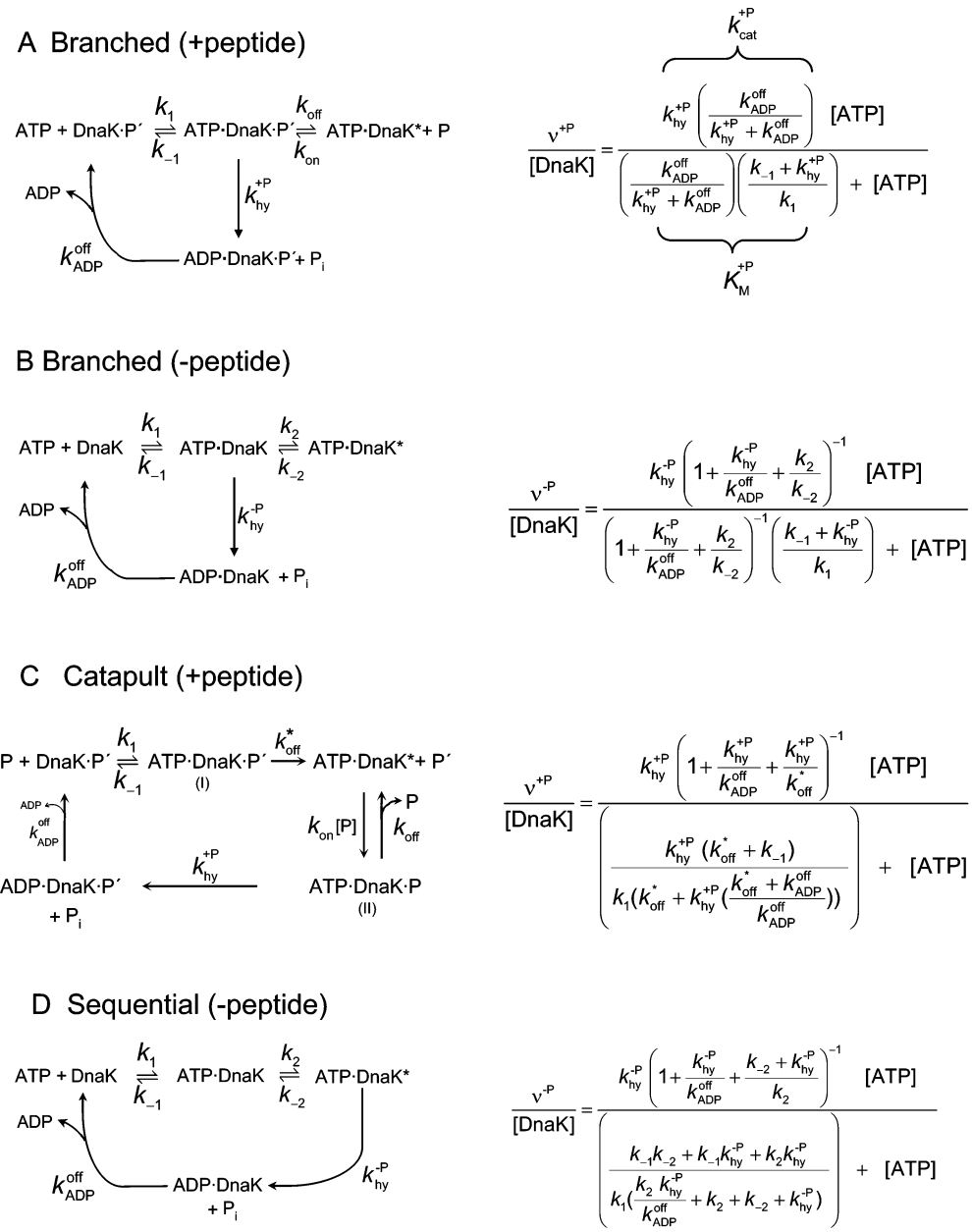

FIGURE 1: Branched mechanism with and without saturating peptide are shown in (A) and (B), respectively. Sequential mechanism with and without saturating peptide are shown in (C) and (D), respectively. In (C), I and II denote different intermediates. The asterisk in ATP·DnaK* denotes decreased fluorescence relative to the other states. P and P′ represent two different conformations of a polypeptide substrate.

coupling between the two domains, as judged by the inability of ATP to trigger the release of bound peptide (and decrease DnaK's tryptophan fluorescence), as well as the inability of peptide to stimulate DnaK-mediated ATP hydrolysis.

Although kinetic analysis has been very useful in showing how nucleotides modulate the conformation and reactivity of Hsp70 chaperones (*7*−*9*, *22*), many different Hsp70 mechanisms have been proposed and few attempts have been made to distinguish between them. In the present study, we have attempted to distinguish between two mechanisms that have been proposed to explain chaperone interactions with ATP and misfolded or unfolded substrates. One of these mechanisms, referred to here as the branched mechanism, contains competing parallel reactions and a ligand-activated molecular switch (Figure 1A) (*23*−*25*), whereas, the other mechanism, referred to as the catapult (Figure 1C), contains sequential reactions, one of which is a unique unidirectional peptide ejection step (*26*). Steady-state ATPase experiments that were conducted in this study support the branched mechanism and rule out the catapult mechanism.

MATERIALS AND METHODS

Protein and Reagents. Reagents were of the highest purity and were purchased from Sigma, unless stated otherwise. DnaK was isolated using ATP-agarose affinity chromatography followed by ion exchange chromatography, as described (*27*). The sample buffer consisted of 25 mM *N*-(2-hydroxyethyl) piperazine-*N*′-2-ethanesulfonic acid (HEPES)/50 mM KCl/5 mM $MgCl_2$/5 mM 2-mercaptoethanol at pH 7.0. The proteins were made nucleotide-free by exhaustive dialysis (16 L of buffer over 4 days) (*27*) or by the method of Gao et al. that employs 5′-adenylyl imidodiphosphate

(AMP−PNP) (*28*) and then stored in the HEPES sample buffering containing 10% glycerol at −80 °C prior to use. The endogenous nucleotide content in DnaK preparations after either of these treatments was estimated by the A_{280}/A_{260} ratio. In every case, $A_{280}/A_{260} = 1.5-1.7$, which indicated that DnaK was nucleotide-free (*29*). Glycerol was removed by an overnight dialysis before using the protein. DnaK was judged to be greater than 95% pure based on Coomassie blue staining of SDS−PA gels.

The p5 peptide was purchased from Genemed Synthesis Incorporated (S. San Francisco, CA), purified to >95% by high performance liquid chromatography, and peptide mass was verified by electrospray mass spectroscopy.

ATPase Activity Measurements. The ATPase assay was performed as described by Karzai and McMacken (*30*). Briefly, the reaction mixture (40 μL) contained 50 nM DnaK (2.0 pmol), 25 mM HEPES/KOH, 11 mM magnesium acetate, 150 mM potassium glutamate at pH 7.6. For the ATP concentration range 5−400 nM, a 500 nM stock solution of ATP (ATP + [α-^{32}P]-ATP) was used (specific activity 100 Ci/mmol). For the ATP concentration range of 600 nM to 17.5 μM, a 50 μM stock solution of ATP (ATP + [α-^{32}P]-ATP) was used (3.6 Ci/mmol). For the ATP concentration range of 100−250 μM, a 2.5 mM stock solution of ATP (ATP +[α-^{32}P]-ATP) was used (2.5 Ci/mmol). Samples were preincubated 2 min at 25 °C prior to the addition of ATP. Aliquots (3 μL) were removed periodically and quenched with 1 μL 0.2 M HCl, and then 2 μL aliquots were subjected to polyethyleneimine (PEI)-cellulose thin-layer chromatography using a 1 M formic acid and 0.5 M lithium chloride mobile phase. Radiolabeled ATP and ADP were detected and quantified using a STORM 860 Phosphorimager. Product formation traces were analyzed by linear-regression to determine the initial rates of ATP hydrolysis (v_0, pmol ADP min^{-1}). Rates were divided by the picomoles of DnaK in the reaction (v_0/[DnaK], min^{-1}). Nonenzymatic hydrolysis of ATP was determined for each experiment and did not exceed 8 ± 1.5% after 4 h incubation. For experiments using the p5 peptide, the p5 peptide concentration was 500 μM.

Curve Fitting and Error Analysis. Least-squares fitting of data and determinations of standard errors of the fitted parameters were conducted using the program KaleidaGraph (Synergy Software, Reading, PA). Errors were propagated according to methods outlined in Bevington (*31*).

RESULTS

The objective of this study was to test two different types of mechanisms, branched and sequential, of chaperone action. In the branched mechanism (Figure 1 A), ATP binds to a DnaK·P complex and forms an intermediate (ATP·DnaK·P), which then undergoes competing parallel reactions that produce products that possess very different kinetic and spectral properties. Hydrolysis yields ADP·DnaK·P, from which peptide dissociation is very slow. Hydrolysis occurs without a spectral change in DnaK. Competing against hydrolysis, a conformational change yields ATP·DnaK*, from which peptide dissociation is quite fast. This conformational change partially quenches the tryptophan fluorescence of DnaK (indicated by an asterisk) (*23*, *24*). In this mechanism, peptide binding reverses the forward conformational change and increases the amount of the intermediate complex, which in turn increases the rate of DnaK-mediated ATP hydrolysis ($= k_{hy}^{+P} \times$ [ATP·DnaK·P]). Two ATP-bound states exist in this mechanism, ATP·DnaK·P and ATP·DnaK*. The companion branched mechanism for the reaction between DnaK and ATP in the absence of peptide is shown in Figure 1B. The ATP-bound intermediate is the branch point for each mechanism.

In the catapult mechanism (Figure 1C), which is a unique form of a sequential mechanism, ATP rapidly binds to a DnaK·peptide complex and forms an intermediate (ATP·DnaK·P)$_I$. A conformational change then occurs that releases the bound peptide and partially quenches the protein's tryptophan fluorescence, forming the low-affinity state (ATP·DnaK*) (*26*). The unique aspect of the catapult mechanism is that this conformational change that releases the bound peptide from the (ATP·DnaK·P)$_I$ intermediate is unidirectional. Peptide substrates can rapidly bind (k_{on}) to and rapidly release (k_{off}) from ATP·DnaK*, and the binding of a peptide molecule to ATP·DnaK* increases the tryptophan fluorescence of the protein and creates a second intermediate (ATP·DnaK·P)$_{II}$. ATP hydrolysis converts this second intermediate to the ADP-bound state. After ADP dissociates, ATP binds and triggers the unidirectional release of the bound substrate peptide (k_{off}^*). This catapult step may occur at a different rate than the reversible transient interaction ($k_{off}^* \neq k_{off}$). Three ATP-bound states exist in the catapult mechanism, (ATP·DnaK·P)$_I$, ATP·DnaK*, and (ATP·DnaK·P)$_{II}$. The companion sequential mechanism for the reaction between DnaK and ATP in the absence of peptide is shown in Figure 1D.

Evidence from pre-steady-state kinetic experiments in support of a bidirectional conformational switch in DnaK (eq 1) was previously reported (*23*).

$$\mathrm{ATP} + \mathrm{DnaK{\cdot}P} \overset{K_1}{\rightleftharpoons} \mathrm{ATP{\cdot}DnaK{\cdot}P} \underset{k_{on}}{\overset{\Delta F\downarrow\ k_{off}}{\rightleftharpoons}} \mathrm{ATP{\cdot}DnaK^*} + \mathrm{P} \quad \Delta F\uparrow \tag{1}$$

One key finding was that for stopped-flow experiments that probed the forward reaction, in which the ATP concentration was varied in one syringe with a fixed concentration of DnaK·peptide complexes in the other syringe, the observed rate (k_{obs}) of ATP-induced fluorescence quenching followed

$$k_{obs} = k_{on}[\mathrm{P}] + \frac{k_{off}[\mathrm{ATP}]}{K_1 + [\mathrm{ATP}]} \qquad \text{(forward reaction)} \tag{2}$$

Another key finding was that for stopped-flow experiments that probed the reverse reaction, in which the peptide concentration was varied in one syringe with a fixed concentration of ATP·DnaK complexes in the other syringe, the observed rate (k_{obs}) of peptide-induced fluorescence increase followed

$$k_{obs} = k_{on}[\mathrm{P}] + k_{off} \qquad \text{(reverse reaction)} \tag{3}$$

The peptide on- and off-rate constants determined from experiments that probed the forward reaction were exactly equal to the peptide on- and off-rate constants determined

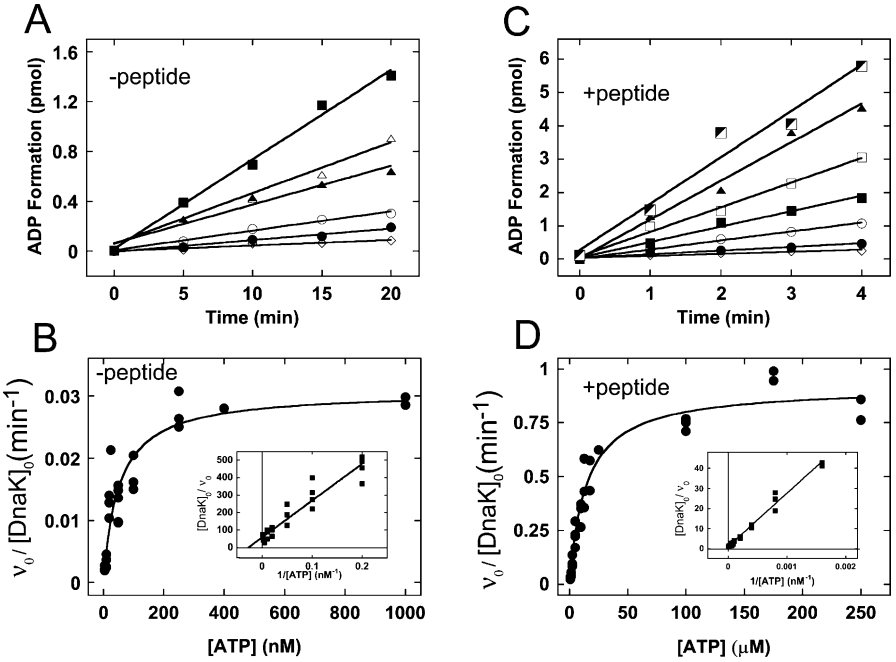

FIGURE 2: Effect of peptide on K_M for ATP. (A) Time courses for the hydrolysis of [α-^{32}P]-ATP by DnaK in the absence of added peptide. ATP was varied over the range 5−250 nM (◇, 5 nM; ●, 10 nM; ○, 20 nM; ▲, 50 nM; △, 100 nM; and ■, 250 nM) at a fixed concentration of DnaK (50 nM; 2.0 pmol per sample). Traces were fit to the equation for a straight line (solid line), where the slope is the velocity, v (pmol ADP min^{-1}). (B) Plot of v_0/[DnaK]$_0$ versus ATP concentration. The solid line is the best fit to the Michaelis-Menton equation and yielded K_M^{-P} and k_{cat}^{-P} equal to 52 ±11 nM and 0.030 ± 0.001 min^{-1} (R = 0.928), respectively. (C) Time courses for the hydrolysis of [α-^{32}P]-ATP by DnaK in the presence of saturating p5 peptide (500 μM). ATP was varied over the range 0.625−250 μM (◇, 0.625 μM; ●, 1.25 μM; ○, 2.5 μM; ■, 5 μM; □, 10 μM; ▲, 12.5 μM; and ◩, 250 μM) at a fixed concentration of DnaK (50 nM; 2 pmol per sample). (D) Plot of v_0/[DnaK]$_0$ versus ATP concentration. The solid line is the best fit to the Michaelis-Menton equation and yielded K_M^{+P} and k_{cat}^{+P} equal to 14.6 ± 1.6 μM and 0.92 ± 0.03 min^{-1} (R = 0.975), respectively. Insets in panels (B) and (D) show double-reciprocal plots.

from experiments that probed the reverse reaction. Although such results support the branched mechanism, they do not disprove the subtly different catapult mechanism. This is because in the catapult mechanism ATP and peptide also induce reciprocal changes in the tryptophan fluorescence of DnaK. Experiments that do not depend on tryptophan fluorescence are needed to distinguish between these two mechanisms.

We posit that the branched and catapult mechanisms can be distinguished via experiments that measure the steady-state ATPase activity of DnaK as a function of the concentration of ATP. That is, although the rate of ATP hydrolysis by DnaK will obey Michaelis-Menton kinetics for each mechanism, the two mechanisms will differ in how peptide affects the K_M for ATP. For example, in the branched mechanism peptide partially reverses the two-step sequential reaction that defines this mechanism (Figure 1A); thus, saturating peptide should increase dramatically the K_M for ATP ($K_M^{+P} \gg K_M^{-P}$). However, in the catapult mechanism peptide drives the reaction forward (Figure 1C), and thus saturating peptide should decrease the K_M for ATP ($K_M^{+P} \ll K_M^{-P}$). Steady-state kinetic experiments were conducted to determine whether saturating peptide increases, decreases, or has no effect on the K_M for ATP.

Measurement of the Rate of DnaK-Mediated ATP Hydrolysis. DnaK-mediated ATP hydrolysis was measured by using [α-^{32}P]-ATP in conjunction with PEI-cellulose chromatography. ATP (ATP/[α-^{32}P]-ATP) was added to a sample of DnaK; aliquots were periodically removed and quenched by the addition of SDS loading buffer. The radiolabeled nucleotides were separated using a PEI-cellulose plate (see Materials and Methods for additional details). Representative time courses for DnaK-mediated ATP hydrolysis in the absence of added p5 peptide, analyzed by linear regression, are shown in Figure 2A. Initial rates of ATP hydrolysis (v_0/[DnaK]$_0$, s^{-1}) are plotted against ATP concentration in Figure 2B. The hyperbolic plot is characterized by k_{cat}^{-P} and K_M^{-P} values of 5.0 ± 0.2 × 10^{-4} s^{-1} and 52 ± 11 nM, respectively. By comparison, K_M^{-P} values for ATP of 19 ± 2 nM (*9*) and 1 μM (*32*) were previously reported for DnaK.

Parallel experiments analyzed the effect of saturating peptide on the rate of DnaK-mediated ATP hydrolysis. The peptide concentration used (500 μM) is much larger than the K_d for p5 binding to ATP-bound DnaK (K_d = 6 μM) (*26*). Representative time courses for DnaK-mediated ATP hydrolysis with saturating p5 peptide, analyzed by linear-regression, are shown in Figure 2C. The plot of v_0/[DnaK]$_0$ versus the concentration of ATP is characterized by k_{cat}^{-P} and K_M^{+P} values of 0.0153 ± 0.0005 s^{-1} and 14.6 ± 1.6 μM, respectively. Saturating peptide therefore increased k_{cat} and K_M 31- and 280-fold, respectively. Such a large increase in K_M supports the branched mechanism and is inconsistent with the catapult mechanism.

Analysis of the Steady-State ATPase Data. To analyze the different mechanisms in Figure 1, the King-Altman method (*33*) was used to derive mathematical expressions for k_{cat} and K_M for each mechanism. The assumptions were that [ATP] > [DnaK], [P] ≫ K_d (dissociation constant for peptide binding to ATP-bound DnaK) or [P] = 0, and k_{ADP}^{on} = 0. Setting this latter rate constant to zero is reasonable because the concentration of ATP is in vast excess over the small

Table 1: Rate Constants for the Various Mechanisms

Saturating Peptide		
catapult (Figure 1 A)		branched (Figure 1 C)
rate constant	comments	rate constant
$k_1 = 1.25 \times 10^5\ M^{-1}\ s^{-1}$	refs *9*, *27*	$k_1 = 1.25 \times 10^5\ M^{-1}\ s^{-1}$
$k_{-1} = 6.0\ s^{-1}$	calculated	$k_{-1} = 793\ s^{-1}$
$k_{hy}^{+P} = 0.050\ s^{-1}$	calculated	$k_{hy}^{+P} = 0.0506\ s^{-1}$
$k_{ADP}^{off} = 0.022\ s^{-1}$	ref *27*	$k_{ADP}^{off} = 0.022\ s^{-1}$
	catapult step ref *26*	$k_{off*} = 6.7\ s^{-1}$
$k_{off} = 5.7\ s^{-1}$	ref *26*	$k_{off} = 6.0\ s^{-1}$
$k_{on} = 1.1 \times 10^6\ M^{-1}\ s^{-1}$	ref *26*	$k_{on} = 1.1 \times 10^6\ M^{-1}\ s^{-1}$
No Peptide		
branched (Figure 1B)		sequential (Figure 1D)
$k_1 = 1.25 \times 10^5\ M^{-1}\ s^{-1}$	refs *9*, *27*	$k_1 = 1.25 \times 10^5\ M^{-1}\ s^{-1}$
$k_{-1} = 6.0\ s^{-1}$	calculated	$k_{-1} = 793\ s^{-1}$
$k_2 = 19\ s^{-1}$	ref *27*	$k_2 = 19\ s^{-1}$
$k_{-2} = 0.02\ s^{-1}$	calculated	$k_{-2} = -3.6 \times 10^{-4}\ s^{-1}$
$k_{hy}^{-P} = 0.5\ s^{-1}$	calculated	$k_{hy}^{-P} = 0.0005\ s^{-1}$
$k_{ADP}^{off} = 0.022\ s^{-1}$	ref *27*	$k_{ADP}^{off} = 0.022\ s^{-1}$

amount of ADP generated in a few cycles. The four Michaelis-Mention equations are given in Figure 1A−D.

We show below that values for k_{hy}^{+P} and k_{-1} in the branched and catapult mechanisms can be calculated using information determined in this and previous studies. For the branched mechanism with saturating peptide (Figure 1A), a calculated value for the intrinsic hydrolysis rate constant k_{hy}^{+P} was obtained from the following equation:

$$k_{cat}^{+P}\ (\text{branched}) = 0.0153\ s^{-1} = \frac{k_{hy}^{+P}\, k_{ADP}^{off}}{k_{ADP}^{off} + k_{hy}^{+P}} \qquad (4)$$

The right-hand side of the above equation is the theoretical expression for k_{cat}^{+P}, which was derived using the King-Altman method (Figure 1A), whereas the left-hand side of the equation is the measured value for k_{cat}^{+P} (Figure 2C,D). Substituting for k_{ADP}^{off} (= 0.022 s^{-1}) (*27*) in the above equation and solving for k_{hy}^{+P} yields 0.0506 s^{-1}. This calculated constant was then used to determine k_{-1}, the rate constant for ATP dissociation from the peptide-bound intermediate. The theoretical relation for K_M^{+P} was set equal to the experimentally determined value for this constant (= 14.6 μM):

$$K_M^{+P}\ (\text{branched}) = 14.6\ \mu M = \left(\frac{k_{-1} + k_{hy}^{+P}}{k_1}\right)\left(\frac{k_{ADP}^{off}}{k_{ADP}^{off} + k_{hy}^{+P}}\right) \qquad (5)$$

Substituting for k_{ADP}^{off} (= 0.022 s^{-1}), k_1 (= 0.125 μM s^{-1}), and k_{hy}^{+P} (= 0.0506 s^{-1}) into the above equation and solving yields $k_{-1} = 6.0\ s^{-1}$. For comparison, the calculated value of the rate constant for ATP dissociation from the intermediate complex of bovine brain Hsc70 is 1.1 s^{-1} (*22*). Rate constants for the branched mechanism with saturating peptide are given in Table 1.

Notice that for the branched mechanism without added peptide (Figure 1B) there are three unknown rate constants (k_{-1}, k_{-2}, and k_{cat}^{-P}) but only two equations, i.e., one equation for k_{cat}^{-P} and another for K_M^{-P}. If it is assumed that ATP dissociates from the peptide-free intermediate complex (ATP·DnaK) with $k_{-1} = 6.0\ s^{-1}$, then values for k_{cat}^{-P} and k_{-2} can be determined. Thus, for the branched mechanism (Figure 1B), the theoretical expression for the k_{cat}^{-P}/K_M^{-P} ratio was used to solve for k_{hy}^{-P}:

$$\frac{k_{cat}^{-P}}{K_M^{-P}}\ (\text{branched}) = \frac{5 \times 10^{-4}\ s^{-1}}{0.052\ \mu M} = \frac{k_{hy}^{-P} k_1}{k_{-1} + k_{hy}^{-P}} \qquad (6)$$

Substituting in the above equation for k_1 (= 0.125 $\mu M^{-1}\ s^{-1}$) and k_{-1} (= 6 s^{-1}) and solving for k_{hy}^{-P} yields 0.5 s^{-1}. It is intriguing that in this mechanism k_{cat}^{-P} (= 5×10^{-4} s^{-1}) is one thousand times smaller than the intrinsic rate constant for DnaK-mediated ATP hydrolysis, k_{hy}^{-P} (= 0.5 s^{-1}).

A calculated value for k_{-2} (= 0.02 s^{-1}) was also obtained after substituting values of known constants into the theoretical expressions for k_{cat}^{-P} or K_M^{-P} (Figure 1B) and solving for this constant. The rate constants associated with the branched mechanism are presented in Table 1.

We pointed out that for the branched mechanism without peptide there are two equations and three unknowns (k_{-1}, k_{-2}, and k_{hy}^{-P}), and that our strategy was to use the calculated value for k_{-1} (= 6.0 s^{-1}), which was determined with saturating peptide, to determine the other two constants. It should be noted that changing k_{-1} leads to new values for k_{-2} and k_{hy}^{-P}. Specifically, decreasing k_{-1} to 3 s^{-1} and using reported values for k_1 (= 0.125 $\mu M^{-1}\ s^{-1}$), k_2 (= 19 s^{-1}), and k_{ADP}^{off} (= 0.022 s^{-1}) leads to k_{-2} and k_{hy}^{-P} equal to 0.04 and 0.25 s^{-1}, respectively. In the analysis, we assumed a value of 6 s^{-1} for k_{-1} but also recognized that a 2-fold decrease in this constant produces a 2-fold increase and decrease in k_{-2} and k_{hy}^{-P}, respectively.

The steady-state ATPase data obtained with saturating peptide was also analyzed in the context of the catapult mechanism (Figure 1C). The theoretical expression for k_{cat}^{+P}(catapult) was set equal to the experimental value for this constant (eq 7), and the equation was used to determine k_{hy}^{+P}. Substituting values for k_{ADP}^{off} (= 0.022 s^{-1}) and k_{off}^{*} (= 6.7 s^{-1}) (*26*) in eq 7 and solving for k_{hy}^{+P} yields 0.0506 s^{-1}.

$$k_{cat}^{+P}\ (\text{catapult}) = 0.0153\ s^{-1} = k_{hy}^{+P}\left(1 + \frac{k_{hy}^{+P}}{k_{ADP}^{off}} + \frac{k_{hy}^{+P}}{k_{off}^{*}}\right)^{-1} \qquad (7)$$

This calculated constant was then used to determine k_{-1}, the rate constant for ATP dissociation from the intermediate. Specifically, the theoretical relation for K_M^{+P} was set equal to the experimentally determined value for this constant (= 14.6 μM):

$$K_M^{+P}\ (\text{catapult}) = 14.6\ \mu M = \frac{k_{hy}^{+P}\,(k_{off*} + k_{-1})}{k_1\left[k_{off*} + k_{hy}^{+P}\left(\frac{k_{off*} + k_{ADP}^{off}}{k_{ADP}^{off}}\right)\right]} \qquad (8)$$

Substituting in the above equation for k_1 (= 0.125 $\mu M^{-1}\ s^{-1}$), k_{ADP}^{off} (= 0.022 s^{-1}), k_{off}^{*} (= 6.7 s^{-1}), and k_{hy}^{+P} (= 0.0506 s^{-1}) and solving for k_{-1} yields 793 s^{-1}.

To complete our analysis, the sequential mechanism was also analyzed to determine values for k_{hy}^{-P} and k_{-2} (Figure 1D), with the assumption that in the absence of peptide k_{-1} also equals 793 s^{-1}. The derived theoretical expressions for k_{cat}^{-P} and K_M^{-P}, set equal to their respective experimental values, are shown below.

$$k_{cat}^{-P}\,(\text{sequential}) = 5 \times 10^{-4}\,s^{-1} = k_{hy}^{-P}\left(1 + \frac{k_{hy}^{-P}}{k_{ADP}^{off}} + \frac{k_{-2} + k_{hy}^{-P}}{k_2}\right)^{-1} \quad (9)$$

$$K_M^{-P}\,(\text{sequential}) = 0.052\ \mu M = \frac{k_{-1}k_{-2} + k_{-1}k_{hy}^{-P} + k_2 k_{hy}^{-P}}{k_1\left(\frac{k_2 k_{hy}^{-P}}{k_{ADP}^{off}} + k_2 + k_{-2} + k_{hy}^{-P}\right)} \quad (10)$$

Substituting values for k_1 (= 0.125 μM^{-1} s^{-1}), k_{-1} (= 793 s^{-1}), k_2 (= 19 s^{-1}), and k_{ADP}^{off} (= 0.022 s^{-1}) into eqs 9 and 10 yields two equations with two unknowns (k_{hy}^{-P} and k_{-2}). Solving the equations one finds that k_{hy}^{-P} and k_{-2} equal 5×10^{-4} s^{-1} and -3.4×10^{-4} s^{-1}, respectively. Notice that in this sequential mechanism, $k_{cat}^{-P} = k_{hy}^{-P}$ (= 5×10^{-4} s^{-1}). Rate constants associated with this mechanism are shown in Table 1 (lower right-hand column).

Simulations. Simulations were conducted using the program KINSIM (*34*) to compare the branched and sequential mechanisms. The rate constants used for the simulations are in Table 1. Simulated steady-state reactions were conducted by varying ATP (0.001−250 μM) with DnaK fixed (0.05 μM). Each simulation produced an ADP formation ([ADP](t) + [ADP·DnaK·±P](t)) trace, and the initial slope of each trace yielded the rate of ATP hydrolysis (v_0). Rates were divided by the concentration of DnaK (v_0/[DnaK]$_0$) and plotted against [ATP]. Reactions were allowed to proceed for 20−80 min (no peptide) or 5 min (excess peptide).

Steady-State: Comparison of the Branched and Sequential Mechanisms (Without Peptide) (Figure 1B,D). This simulation compared the ATPase activity of DnaK according to the branched and sequential mechanisms with the no added peptide condition. The branched mechanism was simulated using $k_1 = 0.125\ \mu M^{-1}\ s^{-1}$, $k_{-1} = 6.0\ s^{-1}$, $k_2 = 19\ s^{-1}$, $k_{-2} = 0.02\ s^{-1}$, $k_{hy}^{-P} = 0.5\ s^{-1}$, and $k_{ADP}^{off} = 0.022\ s^{-1}$ (lower left-hand column, Table 1). The sequential mechanism was simulated using $k_1 = 0.125\ \mu M^{-1}\ s^{-1}$, $k_{-1} = 793\ s^{-1}$, $k_2 = 19\ s^{-1}$, $k_{-2} = 0\ s^{-1}$, $k_{hy}^{-P} = 0.0005\ s^{-1}$, and $k_{ADP}^{off} = 0.022\ s^{-1}$ (lower right-hand column, Table 1). For the sequential mechanism with k_{-1} equal to 793 s^{-1}, we showed that k_{-2} equaled -3.6×10^{-4} s^{-1}; however, out of necessity k_{-2} was set equal to zero in the simulations. For each simulation, at time zero the DnaK concentration was set equal to 0.05 μM, the concentrations of all other species were set equal to zero, and the concentration of ATP was varied from 1 to 1000 nM. The plots of v_0/[DnaK]$_0$ versus ATP concentration, obtained from these two simulations, show that the branched mechanism, but not the sequential mechanism, mimics quite closely the data obtained from experiment (Figure 3A).

Steady-State: Comparison of the Branched and Catapult Mechanisms (Figure 1A,C). This simulation compared the influence of saturating peptide on the ATPase activity of DnaK according to the branched and catapult mechanisms ([P] = 500 μM). The branched mechanism was simulated using $k_1 = 0.125\ \mu M^{-1}\ s^{-1}$, $k_{-1} = 6.0\ s^{-1}$, $k_{off} = 5.7\ s^{-1}$, $k_{on} = 1.1 \times 10^6\ M^{-1}\ s^{-1}$, $k_{hy}^{-P} = 0.0506\ s^{-1}$, and $k_{ADP}^{off} = 0.022\ s^{-1}$ (upper left-hand column, Table 1). The catapult mechanism was simulated using $k_1 = 0.125\ \mu M^{-1}\ s^{-1}$, $k_{-1} = 793\ s^{-1}$, $k_{off*} = 6.7\ s^{-1}$, $k_{off} = 6.0\ s^{-1}$, $k_{on} = 1.1 \times 10^6\ M^{-1}\ s^{-1}$, $k_{hy}^{-P} = 0.0506\ s^{-1}$, and $k_{ADP}^{off} = 0.022\ s^{-1}$ (upper right-hand column, Table 1). At time zero, the DnaK concentration was set equal to 0.05 μM, the concentrations of all other species were set equal to zero, and the concentration of ATP was varied from 1 to 250 μM. The plots of v_0/[DnaK]$_0$ versus ATP concentration, obtained from these two simulations, show that the branched mechanism, but not the catapult mechanism, mimics quite closely the data obtained from experiment (Figure 3B). The combined simulations in Figure 3 show the versatility of the branched mechanism, i.e., it accounts for DnaK's ATPase activity with or without added peptide. In contrast, the catapult and its companion sequential

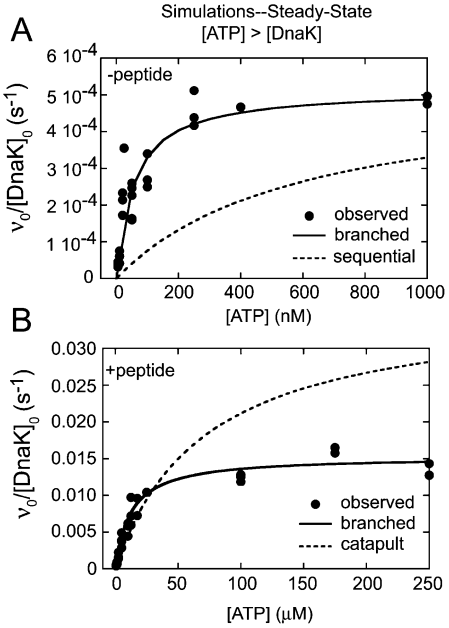

FIGURE 3: Simulated steady-state ATPase activity. (A) Simulations of the branched and sequential mechanisms without added peptide are shown (Figure 1B,D). The rate constants used to simulate the branched mechanism were $k_1 = 0.125\ \mu M^{-1}\ s^{-1}$, $k_{-1} = 6.0\ s^{-1}$, $k_2 = 19\ s^{-1}$, $k_{-2} = 0.02\ s^{-1}$, $k_{hy}^{-P} = 0.5\ s^{-1}$, and $k_{ADP}^{off} = 0.022\ s^{-1}$. The rate constants used to simulate the sequential mechanism were $k_1 = 0.125\ \mu M^{-1}\ s^{-1}$, $k_{-1} = 793\ s^{-1}$, $k_2 = 19\ s^{-1}$, $k_{-2} = 0\ s^{-1}$, $k_{hy}^{-P} = 0.0005\ s^{-1}$, and $k_{ADP}^{off} = 0.022\ s^{-1}$. For each simulation, at time zero [DnaK] = 0.05 μM, the concentrations of all other species were set equal to zero, and [ATP] = 0.001−1.0 μM. Calculated v_0/[DnaK]$_0$ values fall on the hyperbolic curves (–, branched; - - - , sequential). ●, data from Figure 2B. (B) Simulations of the branched and catapult mechanisms with saturating peptide are shown (Figure 1A,C). The rate constants used for the branched mechanism were $k_1 = 0.125\ \mu M^{-1}\ s^{-1}$, $k_{-1} = 6.0\ s^{-1}$, $k_{off} = 5.7\ s^{-1}$, $k_{on} = 1.1 \times 10^6\ M^{-1}\ s^{-1}$, $k_{hy}^{-P} = 0.0506\ s^{-1}$, and $k_{ADP}^{off} = 0.022\ s^{-1}$. The rate constants used for the catapult mechanism were $k_1 = 0.125\ \mu M^{-1}\ s^{-1}$, $k_{-1} = 793\ s^{-1}$, $k_{off*} = 6.7\ s^{-1}$, $k_{off} = 6.0\ s^{-1}$, $k_{on} = 1.1 \times 10^6\ M^{-1}\ s^{-1}$, $k_{hy}^{-P} = 0.0506\ s^{-1}$, and $k_{ADP}^{off} = 0.022\ s^{-1}$. At time zero, the DnaK concentration was set equal to 0.05 μM, the concentrations of all other protein species were set equal to zero, the concentration of ATP was varied from 1 to 250 μM, and [P] = 500 μM. Calculated v_0/[DnaK]$_0$ values fall on the hyperbolic curves (–, branched; ---, catapult). ●, data from Figure 2D.

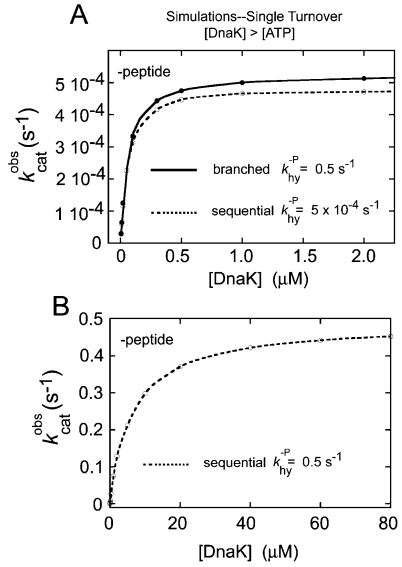

FIGURE 4: Simulated single-turnover ATPase activity. (A) The branched and sequential mechanisms without added peptide (Figure 1B,D) were simulated with the following rate constants: $k_1 = 0.125$ μM^{-1} s^{-1}, $k_{-1} = 6.0$ s^{-1}, $k_2 = 19$ s^{-1}, $k_{-2} = 0.02$ s^{-1}, and $k_{ADP}^{off} = 0.022$ s^{-1} (branched and sequential); and $k_{hy}^{-P} = 0.5$ s^{-1} (branched) or 0.0005 s^{-1} (sequential). For each simulation, at time zero [ATP] = 0.005 μM, the concentrations of all other species were set equal to zero, and [DnaK] = 0.005−2.0 μM. Simulated ADP·DnaK formation traces were fit to a single-exponential function. ATP hydrolysis rates fall on the hyperbolic curves (-●-, branched; - -○- -, sequential). (B) Simulation of the sequential mechanism without peptide with $k_{hy}^{-P} = 0.5$ s^{-1} (Figure 1D). All other rate constants and initial conditions were the same as those described in (A). ATP hydrolysis rates fall on the hyperbolic curve (- -○- -).

mechanism fail to account for DnaK's ATPase activity under these different conditions.

Additional simulations were conducted to highlight the dramatic differences between the branched and sequential mechanisms in the absence of peptide. These simulations were carried out under single turnover conditions, i.e., DnaK was varied (0.005−20 μM) with ATP fixed (0.005 μM). ADP dissociation was not considered. Simulated reactions were allowed to proceed until a plateau was reached, and each reaction produced an ADP·DnaK formation curve that was well fit by a single exponential. Values for k_{cat}^{obs}, obtained from the exponential fits, were plotted against [DnaK].

Single Turnover: Comparison of the Branched and Sequential Mechanisms (Without Peptide) (Figure 1 B,D). This simulation compared the ATPase activity of DnaK according to the branched and sequential mechanisms under single turnover conditions for the no added peptide condition. The only rate constant that differed between the two simulations was k_{hy}^{-P}, which was set equal to 0.5 s^{-1} (branched) or 0.0005 s^{-1} (sequential); otherwise, all other rate constants were identical ($k_1 = 0.125$ μM^{-1} s^{-1}, $k_{-1} = 6.0$ s^{-1}, $k_2 = 19$ s^{-1}, $k_{-2} = 0.02$ s^{-1}, and $k_{ADP}^{off} = 0.022$ s^{-1}). For each simulation, at time zero, the ATP concentration was set equal to 0.005 μM, the concentrations of all other species were set equal to zero, and the concentration of DnaK was varied from 0.005 to 2.0 μM. These two different mechanisms with very different k_{hy}^{-P} values yield almost superimposable plots of k_{cat}^{obs} versus [DnaK] (Figure 4A). For comparison, a simulation was also conducted of the sequential mechanism without peptide in which k_{hy}^{-P} was set equal to 0.5 s^{-1} (Figure 4B); the other rate constants and initial conditions as described above, except DnaK was varied over a larger range. The simulations show that in the absence of peptide the branched mechanism with k_{hy}^{-P} equal to 0.5 s^{-1} yields k_{cat} equal to 0.0005 s^{-1}, and this is true for single turnover and steady-state experiments because the branch point occurs before the ADP dissociation step.

DISCUSSION

The large increase in the K_M for ATP due to saturating peptide supports the branched mechanism of chaperone action (Figure 1A,B). Although the catapult mechanism matches the K_M^{+P} value for ATP (= 14.6 μM) if k_{-1} equals 793 s^{-1}, this value is far too large given that the dissociation of ADP from DnaK does not exceed 127 s^{-1} even when the nucleotide exchange catalyst GrpE is bound to DnaK (*35*). The results in this study support the branched mechanism and rule out the catapult mechanism. Several aspects of this work are discussed below.

A Conformational Equilibrium in the ATPase Domain of DnaK. In our analysis of the steady-state ATPase results, the rate constant for the ATP·DnaK → ATP·DnaK* transition, k_2, equaled 19 s^{-1}. It is important to mention how this constant was determined. Stopped-flow studies have shown that when ATP is mixed with nucleotide and peptide-free DnaK that two distinct phases of tryptophan fluorescence quenching occur (*26*, *27*). The observed rate constant for the rapid phase exhibited a hyperbolic dependence on ATP concentration, with an asymptote[2] equal to 19 s^{-1}, whereas the observed rate constant for the slow phase (0.5−0.7 s^{-1}) exhibited almost no dependence on ATP concentration. In contrast, when ATP is mixed with nucleotide-free DnaK−peptide complexes only one phase of tryptophan fluorescence quenching occurs (*23*). In this case, the observed rate constant exhibits a hyperbolic dependence on ATP concentration, with an asymptote equal to 3−10 s^{-1}. To explain this effect of the peptide substrate on the kinetics of ATP binding, a conformational equilibrium that precedes a two-step sequential reaction was proposed (eqs 11, 12) (*23*, *36*). The asterisk in reaction 12 denotes quenched tryptophan fluorescence compared to the other DnaK states.

$$ {}_{c}\text{DnaK} \underset{k_{co}}{\overset{\text{slow}\ k_{co}}{\rightleftharpoons}} {}_{o}\text{DnaK} \qquad k_{co} \approx k_{oc} \approx 0.67\ \text{s}^{-1} \tag{11}$$

$$ \text{ATP} + {}_{o}\text{DnaK} \underset{k_{-1}}{\overset{k_1}{\rightleftharpoons}} \text{ATP·DnaK} \underset{\Delta\uparrow}{\overset{\Delta F\downarrow\ k_2}{\rightleftharpoons}} \underset{k_{-2}}{} \text{ATP·DnaK*} $$

$$ k_2 = 19\ \text{s}^{-1} \tag{12}$$

It was proposed that the ATPase domain of DnaK slowly opens and slowly closes (eq 11), without causing a spectral changes in the protein, yielding about equal amounts of the two conformations at 25 °C. A closed-to-open equilibrium

[2] The fast phase of ATP-induced tryptophan fluorescence quenching occurs in the second step of reaction 12. The asymptote of the plot of the observed rate of the fast phase versus [ATP] is $k_2 + k_{-2} = 19$ s^{-1}. We reasonably assume that $k_2 \gg k_{-2}$; thus, k_2 was set to 19 s^{-1}.

had been reported for the structurally similar ATP binding domain of hexokinase (*37*). The existence of two conformations of nucleotide-free DnaK was also obtained from a chemical cross-linking study (*38*). When added to an equimolar mixture of these two conformations, ATP rapidly reacts with the open isomer (reaction 12), and this reaction produces the rapid phase of tryptophan fluorescence quenching. The remaining molecules are stalled in the closed conformation and must open before ATP can bind. This slow opening thus causes the slow phase of ATP-induced tryptophan fluorescence quenching. Additional insights into this problem came from a recent NMR investigation that demonstrated the existence of a slow conformational equilibrium ($< 10\ s^{-1}$) in the ATPase domain of *Thermus thermophilus* DnaK (*39*).

It was proposed that the addition of peptide to the system shifts nucleotide-free DnaK molecules to the open conformation ($_c$DnaK + P $\rightleftharpoons$ $_o$DnaK·P), and this abolishes the slow phase of ATP binding (*23*). In this model, in the presence of excess peptide, ATP rapidly binds to DnaK·P complexes in the two-step reaction shown in Figure 1A (or eq 1). This conformational equilibrium in the ATPase domain was not considered in the present analysis because ATP and peptide were in vast excess over DnaK.

This study has revealed new insights into how DnaK hydrolyzes ATP in the absence of polypeptides. The principal discovery was that the branched and sequential mechanisms are indistinguishable under certain conditions. That is, each mechanism mimics the observed steady-state ATPase kinetics and yields k_{cat}^{-P} equal to $0.0005\ s^{-1}$, when the only rate constant that differed between the two mechanisms was k_{hy}^{-P}, which was set equal to $0.0005\ s^{-1}$ and $0.5\ s^{-1}$ in the sequential and branched mechanisms, respectively. Thus, in the sequential mechanism $k_{cat}^{-P} = k_{hy}^{-P}$, whereas in the branched mechanism $k_{cat}^{-P} \ll k_{hy}^{-P}$. Parallel competing reactions produce this large disparity between k_{cat}^{-P} and k_{hy}^{-P}. Specifically, the conformational transition ($19\ s^{-1}$) outcompetes hydrolysis ($0.5\ s^{-1}$), which in turn creates a concentration imbalance, [ATP-DnaK*] $\gg$ [ATP-DnaK], that causes the decrease in the rate of ATP hydrolysis. The expressions derived from the King-Altman analysis (Figure 1) can help us understand the exact relationship between k_{cat}^{-P}, k_{hy}^{-P}, and the other rate constants. For steady-state reactions in the branched pathway without peptide, v_{max}^{-P} depends on [ATP] according to

$$v_{max}^{-P} = \frac{k_{cat}^{-P}[ATP]}{K_M^{-P} + [ATP]} \tag{13}$$

where k_{cat}^{-P} is defined by

$$k_{cat}^{-P} = k_{hy}^{-P}\left(1 + \frac{k_{hy}^{-P}}{k_{ADP}^{off}} + \frac{k_2}{k_{-2}}\right)^{-1} \tag{14}$$

Substituting values for k_{hy}^{-P} ($= 0.5\ s^{-1}$), k_{ADP}^{off} ($= 0.022\ s^{-1}$), k_2 ($= 19\ s^{-1}$), and k_{-2} ($= 0.02\ s^{-1}$) into the right-hand side of eq 14 yields k_{cat}^{-P} equal to $0.0005\ s^{-1}$. In making this calculation, one sees that the k_2/k_{-2} term dominates the others. Another way to see that $k_{cat}^{-P} \ll k_{hy}^{-P}$ in the branched mechanism is to consider single turnover conditions, where k_{cat}^{-P} is defined by

$$k_{cat}^{-P} = k_{hy}^{-P}\left(\frac{k_{-2}}{k_{-2} + k_2}\right) \tag{15}$$

where the term in parentheses is the fraction of molecules that exist as the ATP·DnaK intermediate. With k_2 and k_{-2} equal to 19 and $0.02\ s^{-1}$, respectively, only $\approx$ 1/1000 molecules exist as the intermediate. The rapid forward conformational change and its slow reversal out compete hydrolysis, and this is the reason for the large inequality between k_{cat}^{-P} and k_{hy}^{-P}.

It was well-known that peptide stimulates DnaK-mediated ATP hydrolysis, up to 30-fold, which is what we found (k_{cat}: $5 \times 10^{-4} \rightarrow 1.53 \times 10^{-2}\ s^{-1}$). On the other hand, an unexpected effect is that peptide appears to *decrease* the true rate constant for DnaK-mediated ATP hydrolysis. For example, for the branched mechanism k_{hy}^{-P} equals $0.5\ s^{-1}$, whereas in the presence of saturating peptide it is approximately 10-fold less, $0.0506\ s^{-1}$. One explanation for this seemingly paradoxical effect is that the maximal rate of ATP hydrolysis cannot be achieved when the intermediate is occupied with a peptide. This could be because the ATP·DnaK·P intermediate adopts a subtly different conformation, perhaps involving the ATPase domain, than the peptide-free intermediate (ATP·DnaK). Our analysis leads to the conclusion that peptide has opposing effects in the branched mechanism: (i) Peptide binding drives ATP·DnaK* molecules to the ATP·DnaK·P intermediate, and this increases k_{cat}. (ii) But peptide binding also shifts DnaK into a conformation from which ATP hydrolysis is suboptimal ($k_{hy}^{+P} = 0.0506\ s^{-1}$). The inability of polypeptides themselves to fully activate the ATPase activity of Hsp70s is well-known.

The co-chaperone DnaJ dramatically stimulates DnaK-mediated hydrolysis (*20*, *40*), and it is known that the J domain of DnaJ interacts with a highly conserved site on the ATPase domain of DnaK (*20*, *41*, *42*). Perhaps what DnaJ does is to close the ATPase domain of an ATP-bound DnaK·substrate complex, and the forced closure optimizes ATP hydrolysis ($0.0506 \rightarrow 0.5\ s^{-1}$). In our model of chaperone action, one would predict that in a single turnover experiment employing DnaJ and substrate peptide that $k_{hy}^{+P+J} = k_{hy}^{-P} = 0.5\ s^{-1}$. This value can be compared to values obtained from two studies. In one single turnover study (*40*), it was shown that DnaJ, in the absence of (poly)peptide substrate, increases k_{hy} by 15 000-fold at 5 °C (1.6×10^{-5} [k_{hy}^{-P}] $\rightarrow 0.25\ s^{-1}$ [k_{hy}^{+J}]), and it was estimated that k_{hy}^{+J} could be as large as $5\ s^{-1}$ at 25 °C. In another single turnover study (*20*), it was shown that DnaJ, together with the substrate protein σ^{32}, stimulates DnaK's ATPase activity 1000-fold and that k_{hy}^{+P+J} was between 0.27 and $0.79\ s^{-1}$. Regarding this latter study, the 1000-fold increase in k_{hy} to an average value of $0.53\ s^{-1}$ agrees with the findings from this study.

The analysis presented here raises the possibility that Hsp70 chaperones are weak ATPases because a conformational equilibrium reduces its ATPase activity a 1000-fold from its maximal activity. In this type of system, the co-chaperone DnaJ has two distinct functions (Figure 5). First, DnaJ reverses the intermediate-to-low-affinity state conformational equilibrium in DnaK, which dramatically increases

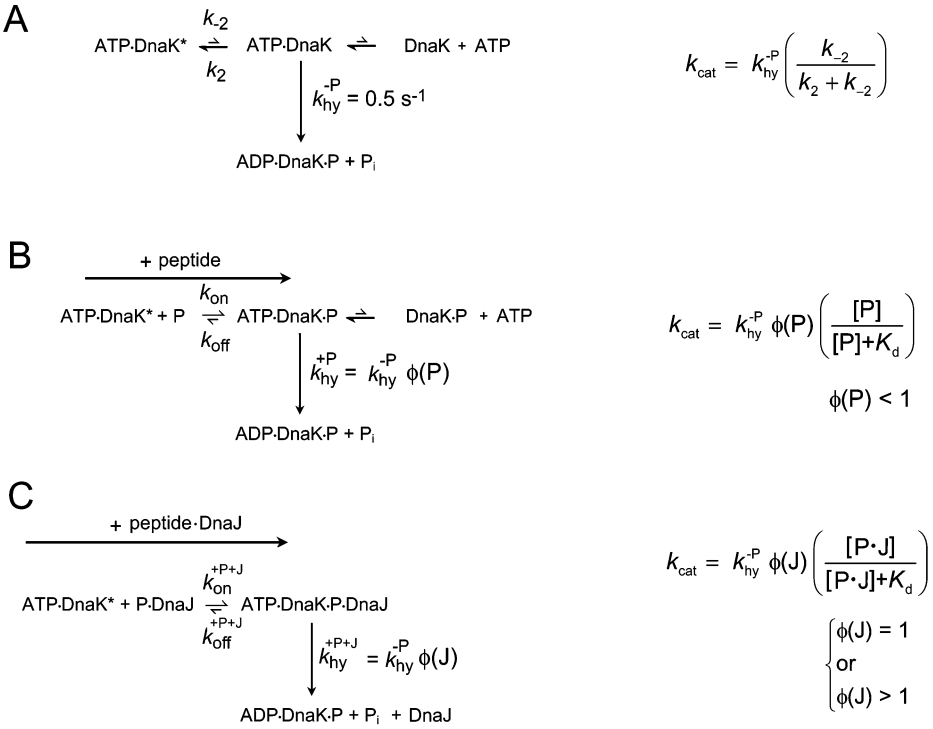

FIGURE 5: ATP hydrolysis in the branched mechanism. Relationships for k_{cat}, which pertain to single turnover conditions, are shown in the right column. (A) No peptide condition. (B) Plus peptide condition. With saturating peptide ([P] $\gg K_d$), the term [P]/([P] + K_d) = 1, and thus $k_{hy}^{+P} = k_{hy}^{-P}\phi(P)$, where $\phi(P) = 0.1$. (C) Peptide plus DnaJ condition. One possibility is that DnaJ drives the two reactions depicted in the figure to completion and $k_{hy}^{+P+J} = 0.5\ s^{-1}$ ($\phi(J) = 1$). The other possibility is that DnaJ drives the two reactions to completion and $k_{hy}^{+P+J} \gg 0.5\ s^{-1}$; in this case, DnaJ is a true catalyst ($\phi(J) > 1$).

the concentration of the intermediate, from which hydrolysis occurs. (Peptides can also do this.) Second, DnaJ promotes a conformational change in the intermediate, for example, forced closure of the ATPase domain or some other conformational change. (Peptides cannot do this.) Each of these processes must occur together to drive DnaK to its maximal rate of ATP hydrolysis, which we suggest is ~0.5 s^{-1}. Note that if DnaJ is a true catalyst as hinted at by Russell et al. (*40*), then a maximal rate of ATP hydrolysis by DnaK greater than 0.5 s^{-1} could be achieved ($k_{hy}^{+P+J} \gg k_{hy}^{-P}$) (Figure 5).

Our model for how DnaJ activates DnaK within the context of the branched mechanism agrees with the bipartite signaling mechanism for DnaJ action proposed by Karzai and McMacken (*30*). They proposed that the stimulation of DnaK-mediated ATP hydrolysis by DnaJ comes about as the result of two separate interactions between these two chaperones. Maximal activation of ATP hydrolysis by DnaK comes about when it simultaneously interacts both with the J domain of DnaJ and with a flexible peptide that can adopt an extended conformation. On the basis of the findings in this study, the flexible peptide shifts the intermediate-to-low-affinity state equilibrium to the intermediate, and the J domain promotes a conformational change in the intermediate that permits hydrolysis to occur at its natural rate in the DnaK system (~0.5 s^{-1} at 25 °C).

A comparison of the rate constants determined for ATP binding to peptide-free DnaK to comparable constants in the peptide-free bovine Hsc70 system shows similar values for the various constants and almost identical K_d values. For example, for DnaK k_1, k_{-1}, k_2, and k_{-2} equal 1.25×10^5 M^{-1} s^{-1}, 6 s^{-1}, 19 s^{-1}, and 0.02 s^{-1}, which yield a K_d of 51 nM ($= k_{-1}/k_1\ k_{-2}/k_2$), whereas for bovine Hsc70, k_1, k_{-1}, k_2, and k_{-2} equal 7×10^5 M^{-1} s^{-1}, 1.1 s^{-1}, 0.66 s^{-1}, and 0.02 s^{-1} (*22*), which yield a K_d of 48 nM. Notice that our calculated K_d (= 51 nM) for ATP interacting with DnaK falls within the range of reported values (1−200 nM) (*8*, *9*, *38*).

In summary, evidence was reported that the Hsp70 DnaK interacts with ATP and peptide substrate according to a branched mechanism rather than a sequential one such as the catapult mechanism. The branched mechanism, which is defined by a DnaK intermediate that undergoes two parallel competing reactions that produce different products, permits an intrinsic rate constant for ATP hydrolysis (k_{hy}^{-P}), in the absence of peptide or DnaJ or both, of up to 0.5 s^{-1}. Thus, we propose that DnaK (and perhaps all Hsp70s) is a "weak" ATPase because of a conformational equilibrium that out competes ATP hydrolysis and dramatically decreases the rate of ATP hydrolysis.

REFERENCES

1. Bukau, B., and Horwich, A. L. (1998) The Hsp70 and Hsp60 chaperone machines, *Cell 92* 351−366.
2. Slepenkov, S. V., and Witt, S. N. (2002) The unfolding story of the *E. coli* molecular chaperone DnaK: Is DnaK a holdase or an unfoldase? *Mol. Microbiol. 45*, 1197−1206.
3. Hartl, F. U., and Hayer-Hartl, M. (2002) Molecular chaperones in the cytosol: from nascent chain to folded protein, *Science 295*, 1852−1858.
4. Zylicz, M., Ang, D., and Georgopoulos, C. (1987) The grpE Protein of *Escherichia coli*, *J. Biol. Chem. 262* (36), 17437−17442.
5. Szabo, A., Langer, T., Schroder, H., Flanagan, J., Bukau, B., and Hartl, F.-U. (1994) The ATP hydrolysis-dependent reaction cycle of the *Escherichia coli* Hsp70 system − DnaK, DnaJ, and GrpE, *Proc. Natl. Acad. Sci. U.S.A. 91*, 10345−10349.

6. Palleros, D. R., Reid, K. L., Shi, L., Welch, W. J., and Fink, A. L. (1993) ATP-induced protein-Hsp70 complex dissociation requires K^+ but not ATP hydrolysis, *Nature 365*, 664−666.
7. Schmid, D., Baici, A., Gehring, H., and Christen, P. (1994) Kinetics of molecular chaperone action, *Science 263*, 971−973.
8. Theyssen, H., Schuster, H.-P., Packschies, L., Bukau, B., and Reinstein, J. (1996) The second step of ATP binding to DnaK induces peptide release, *J. Mol. Biol. 263*, 657−670.
9. Russell, R., Jordan, R., and McMacken, R. (1998) Kinetic characterization of the ATPase cycle of the DnaK molecular chaperone, *Biochemistry 37*, 596−607.
10. Ben-Zvi, A., De Los Rios, P., Dietler, G., and Goloubinoff, P. (2004) Active solubilization and refolding of stable protein aggregates by cooperative unfolding action of individual hsp70 chaperones, *J. Biol.* Chem. *279*, 37298−37303.
11. Shtilerman, M., Lorimer, G. H., and Englander, S. W. (1999) Chaperonin function: folding by forced unfolding, *Science 284*, 822−825.
12. Flaherty, K. M., DeLuca-Flaherty, C., and McKay, D. B. (1990) Three-dimensional structure of the ATPase fragment of a 70K heat-shock cognate protein, *Nature 346*, 623−628.
13. Morshauser, R. C., Wang, H., Glynn, G. C., and Zuiderweg, R. P. (1995) The peptide-binding domain of the chaperone protein HSC 70 has an unusual secondary structure topology, *Biochemistry 34*, 6261−6266.
14. Zhu, X., Zhao, X., Burkholder, W. F., Gragerov, A., Ogata, C. M., Gottesman, M. E., and Hendrickson, W. A. (1996) Structural analysis of substrate binding by the molecular chaperone DnaK, *Science 272*, 1606−1614.
15. Kern, D., and Zuiderweg, E. R. (2003) The role of dynamics in allosteric regulation, *Curr. Opin. Struct. Biol. 13*, 748−757.
16. Flynn, G. C., Chappell, T. G., and Rothman, J. E. (1989) Peptide binding and release by proteins implicated as catalysts of protein assembly, *Science 245*, 385−390.
17. Sadis, S., and Hightower, L. E. (1992) Unfolded proteins stimulate molecular chaperone Hsc70 ATPase by accelerating ADP/ATP exchange, *Biochemistry 31*, 9406−9412.
18. Buchberger, A., Valencia, A., McMacken, R., Sander, C., and Bukau, B. (1994) The chaperone function of DnaK requires the coupling of ATPase activity with substrate binding through residue E171, *EMBO J. 13*, 1687−1695.
19. Suh, W. C., Lu, C. Z., and Gross, C. A. (1999) Structural features required for the interaction of the Hsp70 molecular chaperone DnaK with its cochaperone DnaJ, *J. Biol. Chem. 274*, 30534−30539.
20. Laufen, T., Mayer, M. P., Beisel, C., Klostermeier, D., Mogk, A., Reinstein, J., and Bukau, B. (1999) Mechanism of regulation of hsp70 chaperones by DnaJ cochaperones, *Proc. Natl. Acad. Sci. U.S.A. 96*, 5452−5457.
21. Montgomery, D. L., Morimoto, R. I., and Gierasch, L. M. (1999) Mutations in the substrate binding domain of the *Escherichia coli* 70 kDa molecular chaperone, DnaK, which alter substrate affinity or interdomain coupling, *J. Mol. Biol. 286*, 915−932.
22. Ha, J.-H., and McKay, D. B. (1995) Kinetics of nucleotide-induced changes in the tryptophan fluorescence of the molecular chaperone Hsc70 and its subfragments suggest the ATP-induced conformational change follows initial ATP binding, *Biochemistry 34*, 11635−11644.
23. Slepenkov, S. V., and Witt, S. N. (1998) Peptide-induced conformational changes in the molecular chaperone DnaK, *Biochemistry 37*, 16749−16756.
24. Slepenkov, S. V., and Witt, S. N. (2002) Kinetic analysis of interdomain coupling in a lidless variant of the molecular chaperone DnaK: DnaK's lid inhibits transition to the low affinity state, *Biochemistry 41*, 12224−12235.
25. Slepenkov, S. V., and Witt, S. N. (2003) Detection of a concerted conformational change in the ATPase domain of DnaK triggered by peptide binding, *FEBS Lett. 539*, 100−104.
26. Gisler, S. M., Pierpaoli, E. V., and Christen, P. (1998) Catapult mechanism renders the chaperone action of Hsp70 unidirectional, *J. Mol. Biol. 279*, 833−840.
27. Slepenkov, S. V., and Witt, S. N. (1998) Kinetics of the reactions of the *Escherichia coli* molecular chaperone DnaK with ATP: Evidence that a three-step reaction precedes ATP hydrolysis., *Biochemistry 37*, 1015−1024.
28. Gao, B., Greene, L., and Eisenberg, E. (1994) Characterization of nucleotide-free uncoating ATPase and its binding to ATP, ADP, and ATP analogues, *Biochemistry 33*, 2048−2054.
29. Chaykin, S. (1966) in *Biochemistry Laboratory Techniques*, p 137, John Wiley & Sons, Inc., New York.
30. Karzai, A. W., and McMacken, R. (1996) A bipartite signaling mechanism involved in DnaJ-mediated activation of the *Escherichia coli* DnaK protein, *J. Biol. Chem. 271*, 11236−11246.
31. Bevington, P. R. (1969) *Data Reduction and Error Analysis for the Physical Sciences*, McGraw-Hill, New York.
32. Kamath-Loeb, A. S., Lu, C. Z., Suh, W. C., Lonetto, M. A., and Gross, C. A. (1995) Analysis of three DnaK mutant proteins suggests that progression through the ATPase cycle requires conformational changes, *J. Biol. Chem. 270*, 30051−30059.
33. Segel, I. H. (1993) *Enzyme Kinetics (Behavior and Analysis of Rapid Equilibrium and Steady-State Enzyme Systems*), John Wiley & Sons, New York.
34. Barshop, B. A., Wrenn, R. F., and Frieden, C. (1983) Analysis of numerical methods for computer simulation of kinetic processes: development of KINSIM- -a flexible, portable system, *Anal. Biochem. 130* 134−145.
35. Packschies, L., Theyssen, H., Bucherberger, A., Bukau, B., Goody, R. S., and Reinstein, J. (1997) GrpE accelerates nucleotide exchange of the molecular chaperone DnaK with an associative displacement mechanism, *Biochemistry 36*, 3417−3422.
36. Slepenkov, S. V., Patchen, B., Peterson, K. M., and Witt, S. N. (2003) Importance of DnaK's D and E helices for ATP binding and substrate release, *Biochemistry 42*, 5867−5876.
37. Anderson, C. M., Stenkamp, R. E., McDonald, R. C., and Steitz, T. A. (1978) A refined model of the sugar binding site of yeast hexokinase B, *J. Mol. Biol. 123*, 207−219.
38. Farr, C. D., Slepenkov, S. V., and Witt, S. N. (1998) Visualization of a slow, ATP-induced structural transition in the molecular chaperone DnaK, *J. Biol. Chem. 273*, 9744−9748.
39. Revington, M., Holder, T. M., and Zuiderweg, E. R. (2004) NMR study of nucleotide-induced changes in the nucleotide binding domain of Thermus Thermophilus Hsp70 chaperone DnaK: Implications for the allosteric mechanism, *J. Biol. Chem. 278*, 33958−33967.
40. Russell, R., Karzai, A. W., Mehl, A. F., and McMacken, R. (1999) DnaJ dramatically stimulates ATP hydrolysis by DnaK: Insight into targeting of Hsp70 proteins to polypeptide substrates, *Biochemistry 38*, 4165−4176.
41. Greene, M. K., Maskos, K., and Landry, S. J. (1998) Role of the J-domain in the cooperation of Hsp40 with Hsp70, *Proc. Natl. Acad. Sci. U.S.A. 95*, 6108−6113.
42. Suh, W. C., Burkholder, W. F., Lu, C. Z., Zhao, X., Gottesman, M. E., and Gross, C. A. (1998) Interaction of the Hsp70 molecular chaperone, DnaK, with its cochaperone DnaJ, *Proc. Natl. Acad. Sci. U.S.A. 95*, 15223−15228.

BI050787B